Supplemental Figures

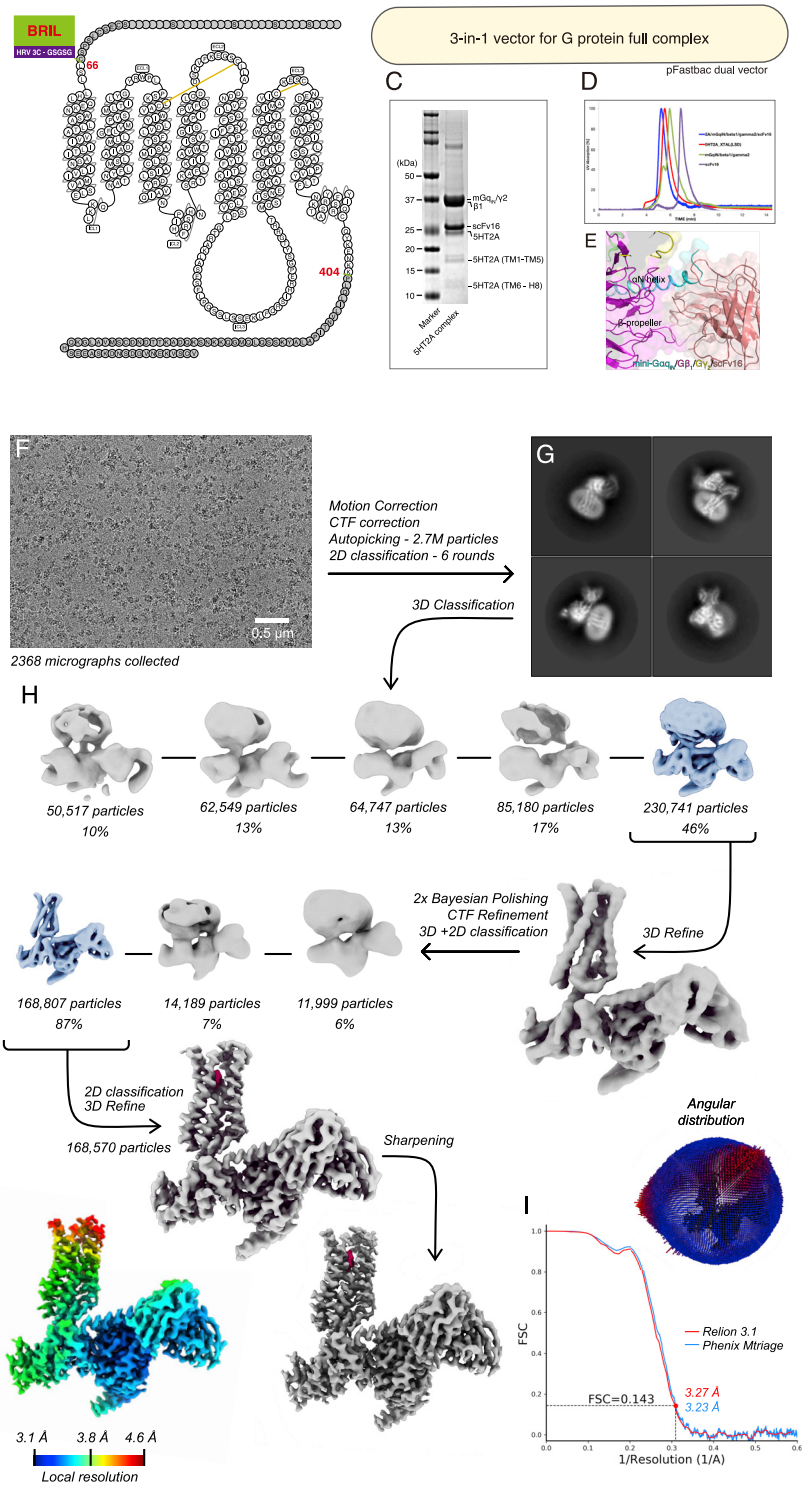

(legend on next page)

Figure S1. Stabilizing a HTR2A(25CN-NBOH)/Gαq Complex and Cryo-EM Workflow for Structure Reconstruction of 5HT2A-MiniG_q Complex, Related to Figure 1

(A) Modified snake diagram from https://gpcrdb.org of an engineered HTR2A construct including truncated N- and C-terminal, as well as N-terminal tagged as HA signal, Flag peptide, His10, TEV protease site, BRIL protein, HRV3C protease site and GSGSG linker. (B) The schematic diagram of a dual vector for the expression of Gαq/β1/γ2 complex. (C) SDS-PAGE showing a complex of HTR2A and Gαq/β1/γ2 after SEC (size exclusion chromatography) (D) aSEC (analytical SEC) showing the retention time of full complex and individual components. (E) The surface view showing the interface between scFv16 (pink) and αN helix of Gαq (cyan)/β-propeller of Gβ1 (magenta) subunits. (F) Representative micrograph of the data collection. (G) Representative 2D averages after 6 rounds of classification, showing distinguishable secondary structure. (H) Data processing workflow, including intermediate maps for 3D classification and refinement, local resolution map computed in Relion 3.0, and the angular distribution of the particle orientations. Gold standard' FSC curves indicate overall nominal resolutions of 3.23 Å using Phenix Mtriage and 3.27 Å using Relion after post-processing.

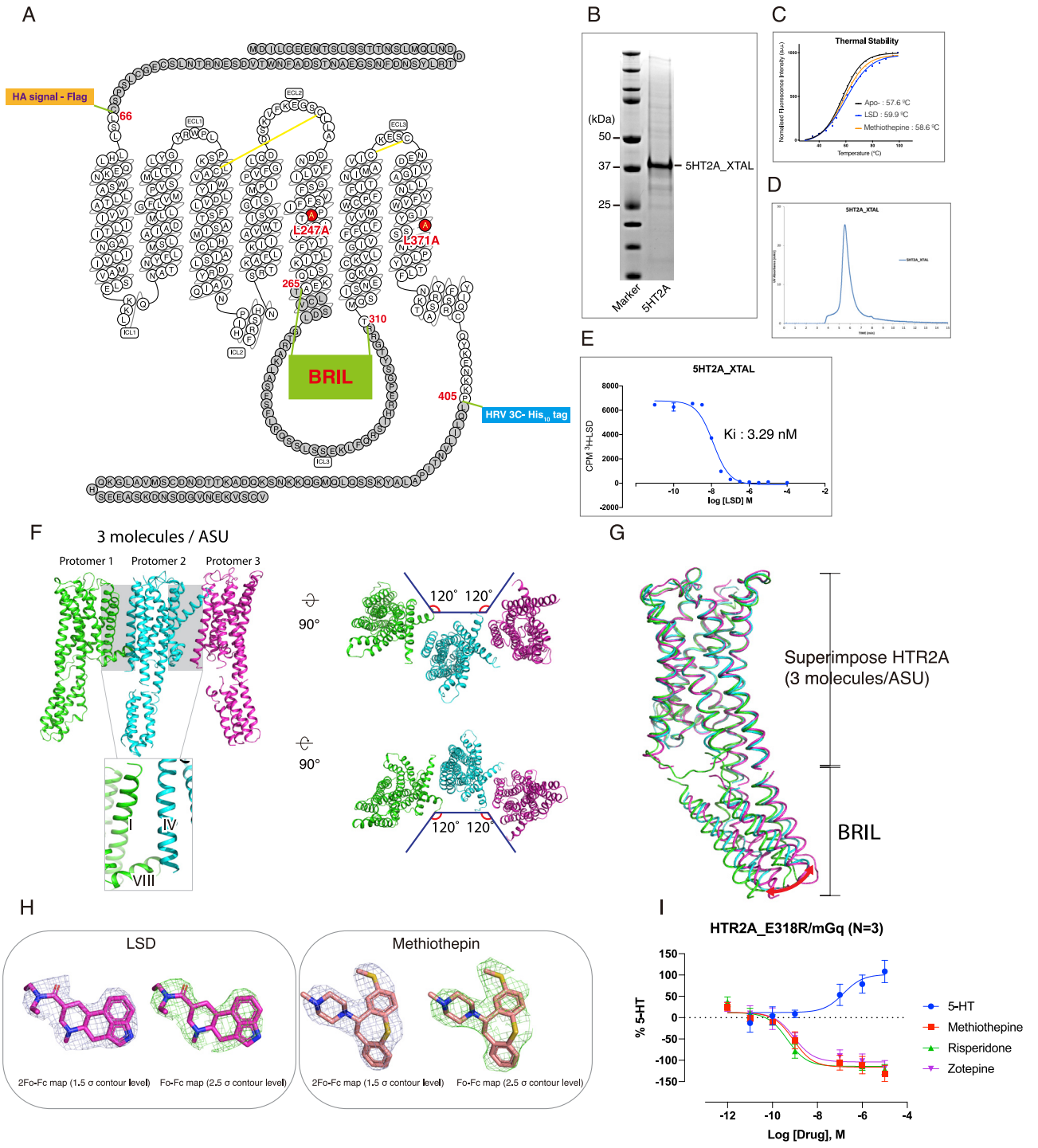

Figure S2. Construct Design, Purification, and Determination of the HTR2A Structure with LSD and Methiothepin, Related to Figure 1

(A) Snake diagram of HTR2A represents the truncation of N- and C-terminal followed by HRV3C cleavage site and His10 tag, and ICL3-BRIL, and two thermostabilized mutations, L247A and L371A. (B) SDS-PAGE of purified HTR2A_XTAL bound to LSD. (C) CPM thermal stability assay of HTR2A at apo-, and different ligands, LSD and methiothepin. (D) aSEC profile of HTR2A_XTAL bound to LSD. (E) Confirmation of HTR2A_XTAL constructs functionality in the binding assay using membrane expressed from *sf9* cell. (F) Three molecules in the asymmetric unit (ASU) and each molecule tilted by 120 degrees. (G) Superimposition of three molecules in templated as HTR2A. (H) Electron density map of LSD (magenta sticks) with 2Fo-Fc (violet mesh) at 1.5σ, and Fo-Fc (green mesh) at 2.5 σ, and methiothepin (pink sticks) with 2Fo-Fc (violet mesh) at 1.5σ and Fo-Fc (green mesh) at 2.5σ. (I) BRET1 HTR2AE318R/mini-Gaq assay showing inverse agonist activity of methiothepin, risperidone, and zotepine. It has previously been reported that HTR2A E318R6.30 mutant is a constitutively active mutant which facilitates the estimation of inverse agonist potency (Shapiro et al., 2002). The pEC_{50} values of methiothepin, risperidone, and zotepine are −9.07 ± 0.15, −9.34 ± 0.15, and −9.04 ± 0.16, respectively. Data represent mean ± SEM from three independent experiments performed in triplicate.

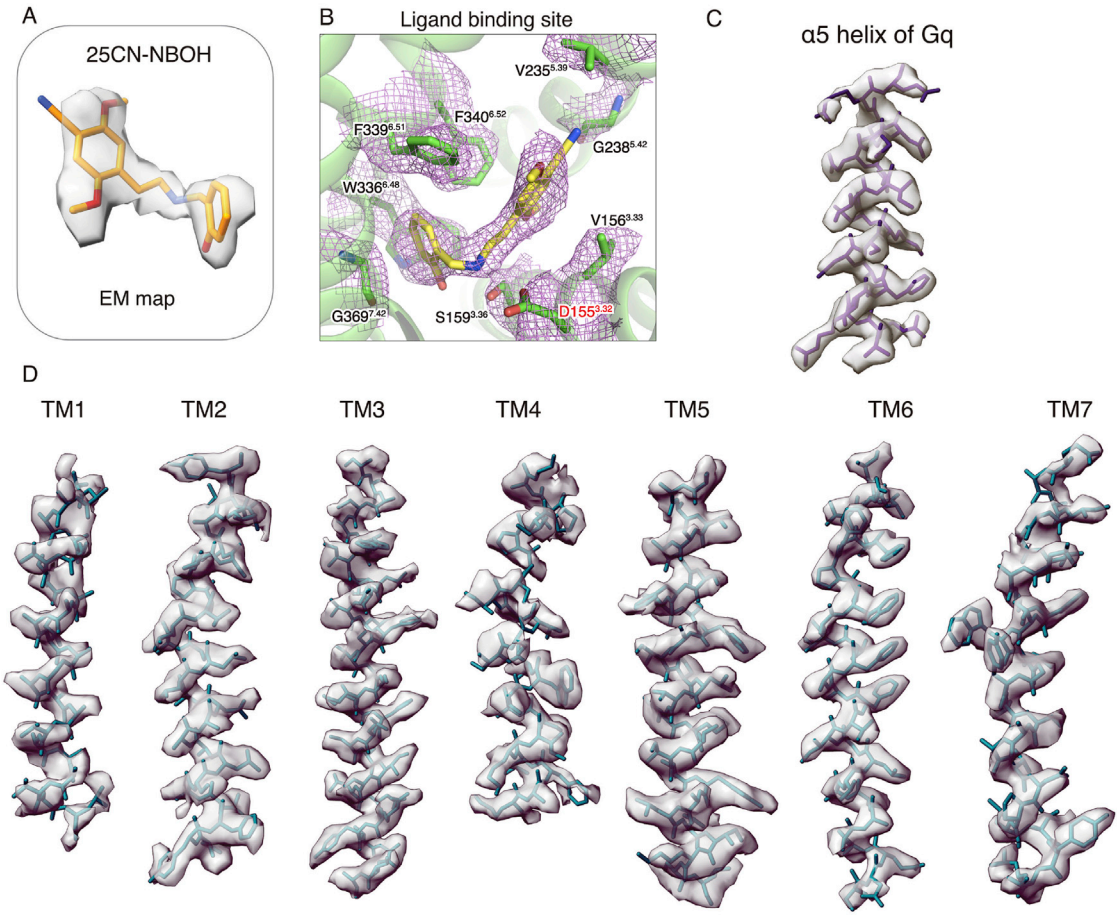

Figure S3. Cryo-EM Maps of HTR2A/25CN-NBOH, Related to Figure 1

The Cryo-EM map of (A) 25CN-NBOH ligand, (B) residues interacting with 25CN-NBOH, (C) α5 Helix of Gαq protein, and (D) TM1-7 of HTR2A.

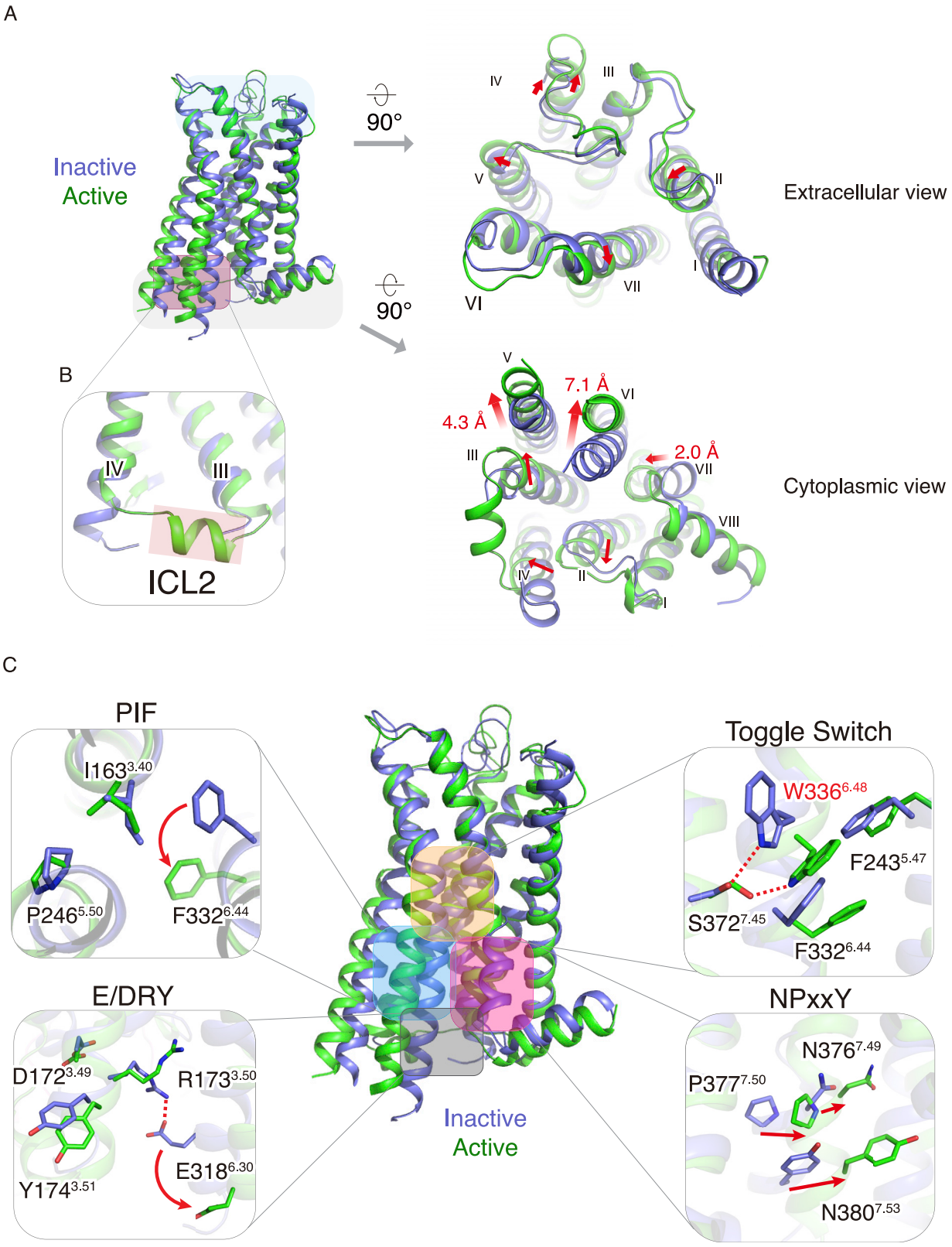

(legend on next page)

Figure S4. Structural Comparison between Inactive and Active State HTR2A, Related to Figure 1

(A, left) Superimposed structures of inactive (violet cartoon) and active (green cartoon) of HTR2A/methiothepin and 25-CN-NBOH structures, respectively. (A, right) the extracellular view shows subtle changes in TMs, and the cytoplasmic view highlights TM5 (4.3 Å) and TM6 (7.1 Å) outward movement and TM7 (2.0 Å) inward movement. Distances were measured between the Cα atoms of A265$^{5.69}$, I316$^{6.27}$ and F383$^{7.56}$. (B) ICL2 of active structure forms helix (green cartoon). (C) Conformational changes between HTR2A/methiothein (inactive) and /25CN-NBOH (active) are highlighted for key representative motifs such as P-I-F, E/DRY, NPxxY, and toggle switch.

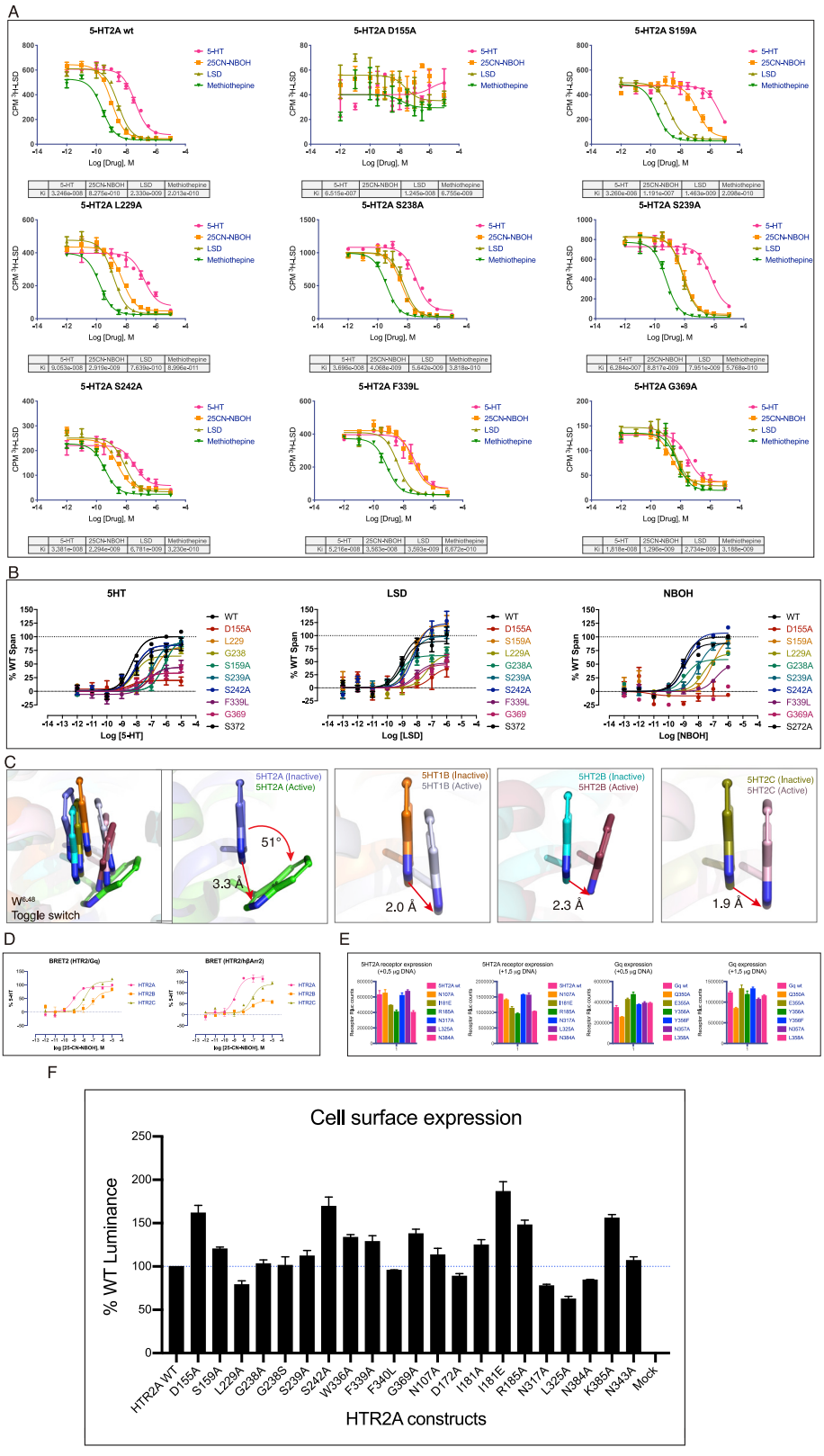

(legend on next page)

Figure S5. Pharmacological Characterization of 25CN-NBOH, LSD, and 5-HT in HTR2A, Related to Figures 3 and 4

(A) Concentration-inhibition curves for 5-HT, 25CN-NBOH, LSD and methiothepin at HTR2A wt and mutants in the ([^{3}H]-LSD, 0.42 nM) binding assay (B) BRET 2 (HTR2A/Gαq) assay of wild-type and mutants involved with ligand-binding pocket with different agonist, 5-HT, LSD, and 25CN-NBOH. (C) The differential translocation of $W^{6.48}$ in HTR2A, 2B, 2C, and 1B. (D) 25CN-NBOH displays HTR2A selectivity over HTR2B or 2C. pEC_{50} values of BRET2 (Gq) with HTR2A, HTR2B and HTR2C are -9.04 ± 0.11, -6.96 ± 0.15, and -7.81 ± 0.10, respectively. pEC_{50} values of BRET1 (hβArrestin 2) with HTR2A, HTR2B and HTR2C are -8.85 ± 0.09, -7.21 ± 0.26, and -6.88 ± 0.11, respectively. (E) Measurement of the expression level of wild-type and mutants HTR2A by Luciferase fluorescence. (F) Measurement of the cell surface expression level of wild-type and mutants HTR2A by ELISA.

A

HTR2A residues		D155	V156	S159	V235	G238	S239	W336	F339	F340	G369	Y370
V-W numbering	Ki (nM)	3.32	3.33	3.36	5.39	5.42	5.43	6.48	6.51	6.52	7.42	7.43
5-HT2A receptor	2.2	D	V	S	V	G	S	W	F	F	G	Y
5-HT2B receptor	58	D	V	S	M	G	S	W	F	F	G	Y
5-HT2C receptor	49.8	D	V	S	V	G	S	W	F	F	G	Y
5-HT1A receptor	<50%	D	V	C	T	S	T	W	F	F	G	Y
5-HT1B receptor	<50%	D	I	C	T	S	T	W	F	F	G	Y
5-HT1D receptor	<50%	D	I	C	T	S	T	W	F	F	G	Y
5-HT1E receptor	<50%	D	M	C	T	S	T	W	F	F	G	Y
5-HT1F receptor	<50%	D	I	C	T	S	T	W	F	F	G	Y
5-HT4 receptor	<50%	D	V	T	A	C	S	W	F	F	G	Y
5-HT5A receptor	<50%	D	V	C	A	S	T	W	F	F	G	Y
5-HT6 receptor	573	D	V	C	V	A	S	W	F	F	G	Y
5-HT7 receptor	<50%	D	V	C	T	S	T	W	F	F	G	Y
M1 receptor	<50%	D	Y	S	T	T	A	W	Y	N	C	Y
M2 receptor	<50%	D	Y	S	T	T	A	W	Y	N	C	Y
M3 receptor	<50%	D	Y	S	T	T	A	W	Y	N	C	Y
M4 receptor	<50%	D	Y	S	T	T	A	W	Y	N	C	Y
M5 receptor	<50%	D	Y	S	T	T	A	W	Y	N	C	Y
α1A-adrenoceptor	<50%	D	V	C	V	S	A	W	F	F	G	Y
α1B-adrenoceptor	<50%	D	V	C	A	S	S	W	F	F	G	Y
α1D-adrenoceptor	<50%	D	V	C	A	S	S	W	F	F	G	Y
α2A-adrenoceptor	803	D	V	C	V	S	C	W	F	F	G	Y
α2B-adrenoceptor	1,226	D	V	C	I	S	S	W	F	F	G	Y
α2C-adrenoceptor	543	D	V	C	I	S	C	W	F	F	G	Y
β1-adrenoceptor	<50%	D	V	V	A	S	S	W	F	F	G	Y
β2-adrenoceptor	1,609	D	V	V	A	S	S	W	F	F	G	Y
β3-adrenoceptor	<50%	D	V	V	V	S	S	W	F	F	G	W
D1 receptor	<50%	D	I	S	A	S	S	W	F	F	G	Y
D2 receptor	<50%	D	V	C	V	S	S	W	F	F	G	Y
D3 receptor	<50%	D	V	C	V	S	S	W	F	F	G	Y
D4 receptor	<50%	D	V	C	V	S	S	W	F	F	G	Y
D5 receptor	<50%	D	I	S	A	S	S	W	F	F	G	W
H1 receptor	<50%	D	Y	S	K	T	A	W	Y	F	G	Y
H2 receptor	1,505	D	V	C	G	D	G	W	Y	F	G	Y
H3 receptor	<50%	D	Y	C	L	A	S	W	Y	T	L	W
H4 receptor	<50%	D	Y	C	L	T	S	W	Y	S	Q	W
δ opioid receptor	<50%	D	Y	M	K	V	F	W	I	H	G	Y
K opioid receptor	<50%	D	Y	M	K	V	F	W	I	H	G	Y
μ opioid receptor	<50%	D	Y	M	K	V	F	W	I	H	G	Y

B

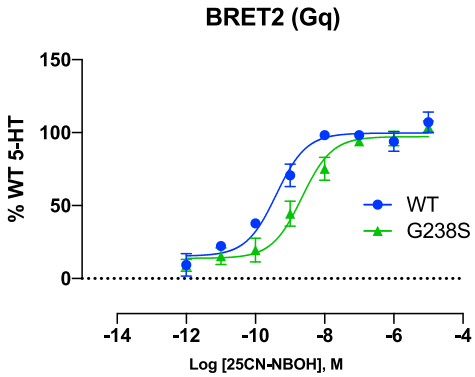

C

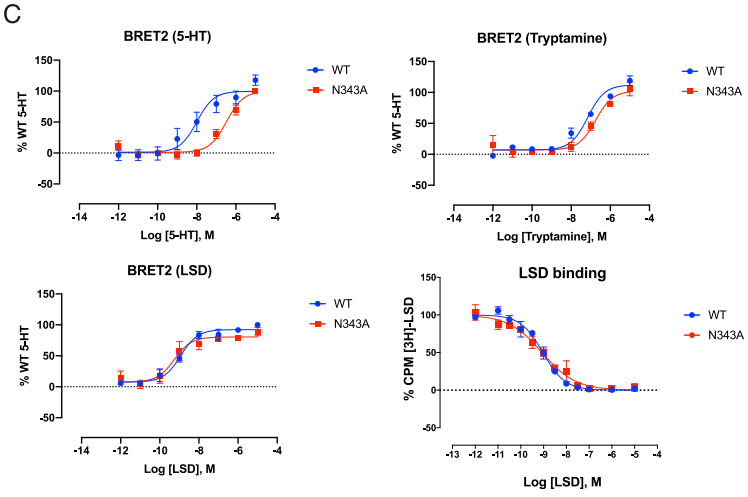

D

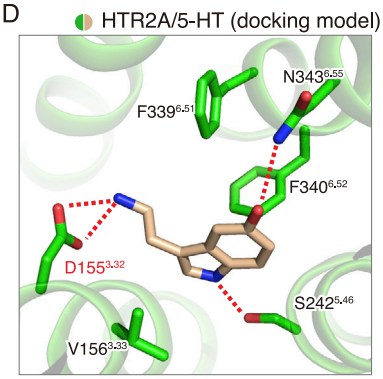

E

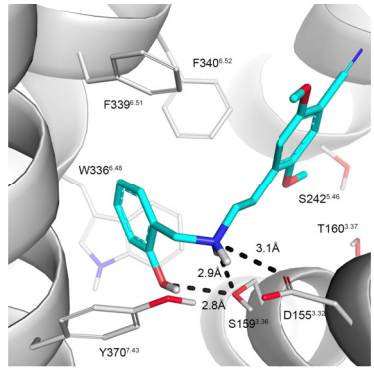

F

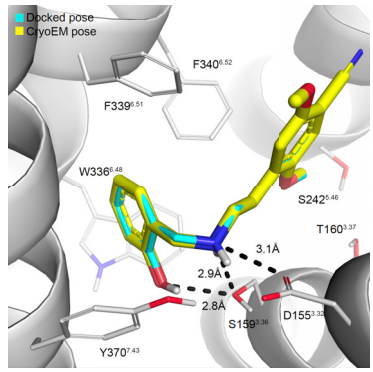

(legend on next page)

Figure S6. 25CN-NBOH Binds Specifically to the HTR2 Subtype with Preference for HTR2A, Related to Figures 3 and 4

(A) Ki values of 25CN-NBOH for all aminergic receptors from the literature (Halberstadt et al., 2016) and the sequence alignment of residues involved in the binding of 25CN-NBOH in HTR2A. The gray color represents conserved residues and < 50% represents less than 50% displacement at 10^{-6} M. (B) The BRET 2 (Gq dissociation) assay of HTR2A wt and G238S mutant showing 6-fold decrease potency of G238S. pEC_{50} of wild-type and G238S are -9.40 ± 0.10 and -8.66 ± 0.10, respectively. (C) The detailed view of 5-HT docking model (stick, ivory color) and HTR2A (green). (D) The BRET 2 results of 5-HT (top left), tryptamine (top right) and LSD (bottom left) in wild-type and N343A mutant showing N343 affects 5-HT with no effect on tryptamine. The binding result (bottom right) of LSD in wild-type and N343A mutant. (E) The docked pose of 25-CN-NBOH in HTR2A, showing key hydrogen bonds as dashed lines (ligand carbons cyan, nitrogens blue, oxygens red, hydrogens white; receptor carbons in gray). (F) The docked pose (carbons in cyan) superposes with that determined by cryo-EM (carbons in yellow) with an r.m.s.d of 0.16Å.

A

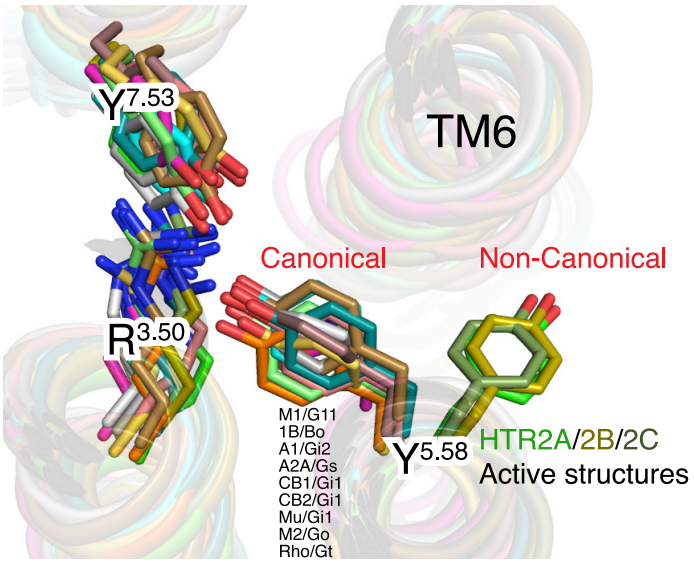

B

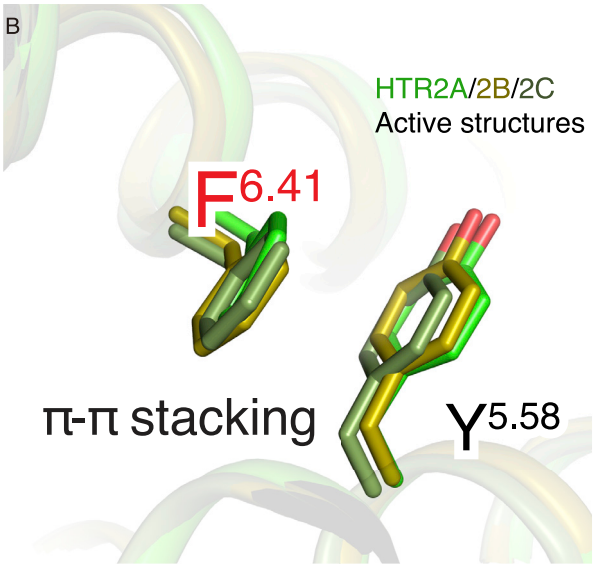

C

Receptors	6.41
5-HT2A receptor	F
5-HT2B receptor	F
5-HT2C receptor	F
5-HT1A receptor	M
5-HT1B receptor	L
5-HT1D receptor	L
5-HT1E receptor	L
5-HT1F receptor	L
5-HT4 receptor	M
5-HT5A receptor	I
5-HT6 receptor	L
5-HT7 receptor	V
M1 receptor	L
M2 receptor	L
M3 receptor	L
M4 receptor	L
M5 receptor	L
α1A-adrenoceptor	V
α1B-adrenoceptor	V
α1D-adrenoceptor	V
α2A-adrenoceptor	I
α2B-adrenoceptor	I
α2C-adrenoceptor	M
β1-adrenoceptor	M
β2-adrenoceptor	M
β3-adrenoceptor	M
D1 receptor	M
D2 receptor	L
D3 receptor	L
D4 receptor	V
D5 receptor	M
H1 receptor	M
H2 receptor	M
H3 receptor	V
H4 receptor	L
TA1 receptor	M

D

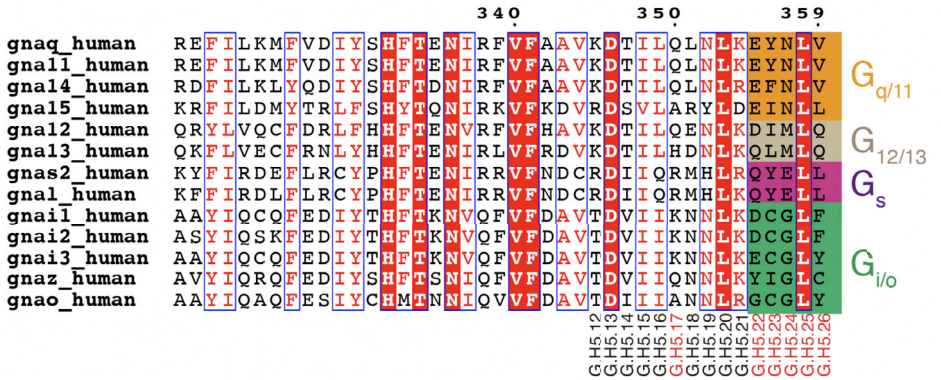

(legend on next page)

Figure S7. $Y^{5.58}$ of HTR2A, HTR2B, and HTR2C Shows Distinct Orientation, Related to Figure 4

(A) Superimposed active structures of HTR2A/Gq, HTR2B, HTR2C, M1/G11, HTR1B/Go, A1/Gi2, A2A/Gs, CB1/Gi1, CB2/Gi1, Mu/Gi1, M2/Go, and Rho/Gt. $Y^{5.58}$, $R^{3.55}$, and $Y^{7.53}$ are highlited with sticks. (B) $F^{6.41}$ and $Y^{5.58}$ fo HTR2s (2A, 2B, and 2C) forms pi-stacking interaction. (C) Sequence alignment of aminergic receptors in position 6.41. Only $F^{6.41}$ (green color) of HTR2s is highly conserved. (D) Sequence alignment of α5 helix of Gα subunits.